Construction and Building Materials 395 (2023) 132306

Contents lists available at ScienceDirect

Construction and Building Materials

journal homepage: www.elsevier.com/locate/conbuildmat

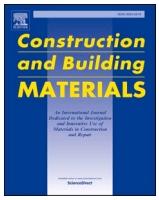

Microcrack monitoring and fracture evolution of polyolefin and steel fibre concrete beams using integrated acoustic emission and digital image correlation techniques

Shahzad Ashraf, Magdalena Rucka *

Department of Mechanics of Materials and Structures, Faculty of Civil and Environmental Engineering, Gdańsk University of Technology, Narutowicza 11/12, 80-233 Gdańsk, Poland

ARTICLE INFO

Keywords:
Fracture monitoring
Fibre-reinforced concrete
Acoustic emission (AE)
Digital image correlation (DIC)

ABSTRACT

The use of polymer and steel fibres in plain concrete appears to be an excellent solution for limiting crack propagation and improving the post-ductility performance of concrete structures. Based on this premise, this study investigated the fracture evolution of polyolefin fibre-reinforced concrete (PFRC) and steel fibre-reinforced concrete (SFRC) specimens through the integrated application of two diagnostic techniques, acoustic emission (AE) and digital image correlation (DIC), under three-point bending tests. Based on the processing of AE signals, different AE statistical parameters such as the cumulative number of hits, amplitude distribution, and some representative analysis methods including the b-value method, Ib-value method, and AE intensity analysis methods were selected to analyse the early detection of cracking and post-cracking behaviour in PFRC vs SFRC specimens during mechanical degradation. Simultaneously, the DIC technique was used to validate the fracture evolution of the AE results. Furthermore, to verify the reliability of the AE and DIC results, the damage localisation and fracture evolution of the PFRC versus SFRC specimens were confirmed by integrating the AE fracture energies and DIC outcomes. The tests and analysed results showed that the addition of steel fibres to plain concrete significantly improved the ability to restrict crack propagation and provided higher post-cracking resistance compared to PFRC specimens owing to their stronger fibre–matrix bonding, effective fibre bridging, and crack-arresting mechanism. The present study indicates that the combined AE and DIC techniques are highly effective for the early detection of damage and ductility performance in fibre-reinforced concrete structures.

1. Introduction

Concrete is one of the most popular construction materials used in all corners of the globe due to its ability to withstand compression, malleability, and cost-effectiveness [1,2]. The main weaknesses of concrete include intrinsic brittleness, weak tensile strength and low crack resistance leading to a drop in the fracture strength once cracking has started [3,4,5]. Concrete fracture is a multi-scale phenomenon that commences with the formation and propagation of micro-cracks and progresses to the development and propagation of macro-cracks, resulting in catastrophic failure [6]. Significant progress has recently been achieved by incorporating various fibres into concrete mixes, such as carbon fibre [7], steel fibres [8,9,10], or polymer fibres [11,12], which offers a productive way to avoid concrete brittleness and enhance the mechanical properties of the fibre-reinforced concrete (FRC). In addition, the fibre bridging and intermeshing effect of the coarse aggregate reduces the activity of concrete micro-cracks at an early age and delays the formation of macro-cracks [13,14]. In order to enhance the durability of load-bearing concrete structures and thus ensure the safety of use, the topic of evaluation of cracking patterns is constantly investigated in the field of civil engineering [15]. Recently, many non-destructive testing (NDT) techniques have been developed for monitoring crack development and early crack detection, including optical and ultrasonic wave-based methods. The acoustic emission (AE) [16,17,18] and digital image correlation (DIC) [19,20] techniques have often been widely used to evaluate the fracture process of quasi-brittle materials during mechanical degradation. Both AE and DIC techniques are oriented on continuous and real-time data acquisition during the fracture process, allowing the formation and progression of microcracks to be monitored during the loading process.

* Corresponding author.
E-mail addresses: shahzad.ashraf@pg.edu.pl (S. Ashraf), magdalena.rucka@pg.edu.pl (M. Rucka).

https://doi.org/10.1016/j.conbuildmat.2023.132306
Received 17 February 2023; Received in revised form 28 April 2023; Accepted 24 June 2023
Available online 1 July 2023

Monitoring of the fracture behaviour of fibre-reinforced cement composites has received considerable attention in previous research. Rucka et al.[19] used digital image correlation and ultrasonic testing to analyze the damage progression in concrete beams reinforced with polyolefin fibres. They came to the conclusion that phase changes and ultrasonic wave energy can be used as damage indicators in polyolefin fibre-reinforced concrete. Xu et al. [21] investigated the damage evolution of polypropylene fibre-reinforced concrete subjected to monotonic and cyclic loading using the AE technique. They concluded that shear cracking dominates the damage evolution in polypropylene fibre-reinforced concrete. Logoń and Schabowicz [22] used AE techniques to distinguish microcracking events in polypropylene fibre reinforcement during a four-point bending test. Logoń [23] investigated the use of the AE approach to identify the cause of failure in quasi-brittle concrete specimens with dispersed polypropylene fibres. He concluded that the analysis of 2D and 3D acoustic spectra could help to identify and explain the failure process in fibre-reinforced concrete elements. Ren et al. [6] employed Brazilian disk splitting tests and acoustic emission (AE) techniques to examine the damage behaviour of steel fibre-reinforced concrete with different steel fibre contents. The mechanical deterioration of concrete specimens with and without chemically treated steel fibres was investigated by Aggelis et al. [24] using the acoustic emission (AE) technique in a four-point bending test. In order to understand the failure mechanism of steel fibre-reinforced coal gangue concrete. Cai et al.[25] introduced a damage evolution model and examined the cracking characteristics using the acoustic emission (AE) technique. Liu et al. [7] studied the fracture phenomena in coral concrete reinforced with different carbon fibre dosages using the DIC method. They analysed that the application of DIC enabled them to characterise three phases (micro-crack commencement, the macrocrack progression, and the major crack growth) of the flexural damage process. The fracture processes in plain concrete and concrete with recycled steel fibres were examined by Skarżyński and Suchorzewski [26]. They used DIC and X-ray micro-computed tomography techniques to analyze the fracture process on the external surfaces and inside the tested specimens. Alam et al. [27] used the DIC and AE techniques to investigate the effect of structure size on cracking in reinforced concrete beams. Boniface et al. [28] investigated the accuracy of AE source localisation in concrete to determine the fracture characteristics and used the DIC technique to validate the comparative results. Zhou et al. [29] utilized the AE approach in conjunction with the DIC technique in order to simultaneously monitor the compressive behaviour of multi-delaminated composites. The results showed that the AE parameters were closely related to the degradation process of composite materials, and the DIC findings represented severe damage inside the multi-delaminated composites.

2. Significance of the research

As mentioned above, numerous studies have investigated the mechanical performance, micro-cracking behaviour, and structural applications of polymer and steel fibre-reinforced composites in various types of concrete structures using digital image correlation and acoustic emission techniques. However, limited attention has been paid to the fracture evolution of fibre-reinforced concrete (PFRC) using combined AE and DIC techniques. Furthermore, there has been no significant investigation into the comparison of polyolefin fibre-reinforced concrete (PFRC) and steel fibre-reinforced concrete (SFRC) specimens using both inspection approaches to characterise the fracture process simultaneously. It is worth noting that PFRC and SFRC could serve as alternatives to normal Portland cement concrete in hot and cold regions where dry shrinkage control and crack initiation delay are critical, as they can provide higher durability and fracture resistance. To address this knowledge gap, the present study undertakes a comprehensive analysis of the characterization of the fracture process in a non-invasive manner.

The present paper is experimentally oriented. Three-point bending tests were performed on concrete specimens reinforced with polyolefin and steel fibre contents of 0.3% and 0.6%, respectively. The non-invasive inspection was based on the simultaneous acquisition of elastic wave signals and photographs of mechanically degraded specimens. The main objective is to better understand the mechanical behaviour of fibre-reinforced concrete structures under mechanical degradation. This knowledge is important for enhancing the safety of concrete structures subjected to various loading conditions, such as severe dry shrinkage, freeze–thaw resistance, flexural bending, compression or impact loading. Summarizing, the current experimental study includes the following novel elements:

1) Detailed and thorough experimental investigations and analyses of fracture evaluation in bending beams reinforced with polyolefin and steel fibres.
2) Integration of DIC and AE techniques to provide a state-of-the-art solution for real-time microcrack monitoring as well as increase the accuracy and efficiency of evaluating fibre-reinforced concrete structures.
3) Analysis of the influence of the amount and type of fibres on the possibility of early detection of cracks using combined AE and DIC techniques.

3. Materials and methods

3.1. Specimens and mixtures

All specimens were manufactured based on the same concrete mixture composed of cement CEM I 42.5R (380 kg/m^3), water (165 kg/m^3), aggregate 0/2 mm (648 kg/m^3), aggregate 2/8 mm (426 kg/m^3), aggregate 8/16 mm (754 kg/m^3), and super-plasticizer (0.8% of the cement content). Five different mixtures were produced. The first mixture was without fibres, i.e. made of plain concrete (PC). The other mixtures contained the addition of polyolefin fibres (PF) and steel fibres (SF), in the amount of 0.3% and 0.6% in the relation to the total volume of concrete. The fibres used in the study are shown in Fig. 1. The 24 mm long polyolefin fibres were produced as twisted bundles. The steel fibres with a length of 25 mm were produced with hooked ends. The properties of fibres are given in Table 1. For each of the five concrete mixtures prepared, the compressive strength determined for the cubic samples with dimensions of 15x15x15 cm^3 as well as elastic modulus were measured. The results are given in Table 2.

The experimental analysis was carried out on five prismatic beams of a length of 160 mm and a cross-section of 40 mm × 40 mm (Fig. 2): plain concrete (PC) specimen, two steel-fibre reinforced concrete (SFRC)

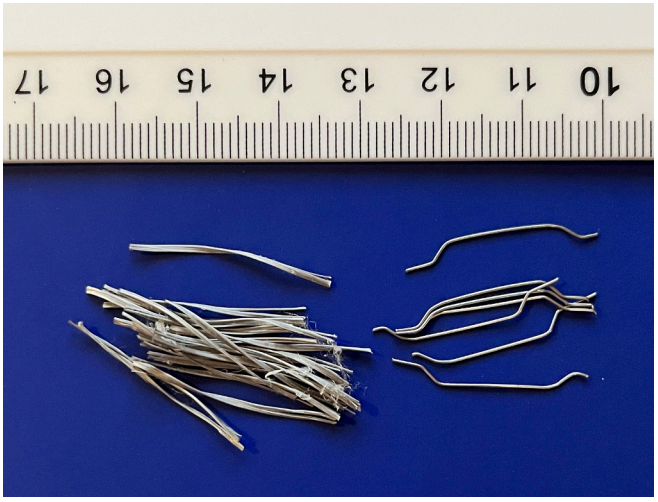

Fig. 1. Photograph of polyolefin fibres (left) and steel fibres (right).

Table 1
Properties of polyolefin and steel fibres.

Type of fibres	Length [mm]	Diameter [mm]	Tensile strength [MPa]	Elastic modulus [GPa]
polyolefin	24	0.45	600	5
steel	25	0.5	2200	200

Table 2
Compression strength of the 15x15x15 cm^3 cubes and elastic modulus.

Mixture	Compression strength [MPa]	Elastic modulus [GPa]
Plain concrete	66.1	40.3
0.3% polyolefin fibres	56.1	39.7
0.6% polyolefin fibres	57.8	39.9
0.3% steel fibres	70.3	40.1
0.6% steel fibres	77.4	43.6

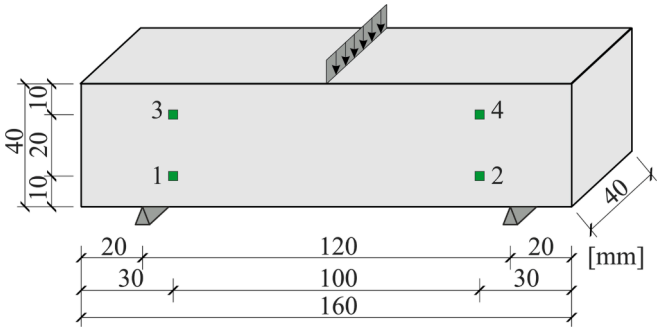

Fig. 2. The geometry of the concrete beam with the location of AE sensors (no. 1–4).

specimens and two polyolefin-fibre reinforced concrete (PFRC) specimens.

3.2. Experimental setup and procedure

The investigations included monitoring the fracture process in a bending test. The experimental setup is shown in Fig. 3. Three-point bending was performed using a Zwick/Roell Z10 universal testing machine (UTM). The beam was placed on linear supports spaced 120 mm apart. A preload of 50 N was applied, and then bending was conducted with a constant mid-span displacement of 0.1 mm/min. During the bending process, crack evolution was characterised using integrated acoustic emission (AE) and digital image correlation (DIC) techniques. Acoustic emission signals were recorded by four multilayer piezoelectric transducers, mounted on the front surface of the beam in the arrangement shown in Fig. 2. The transducers were located outside the area of the expected crack initiation. Data acquisition was performed using the Vallen AE system, with a sampling rate of 10 MHz and a threshold of 34 dB. Images of the front surface of the beams were taken every 1 s using ARAMIS MC 3D 12 M.

3.3. Digital image correlation

Digital Image Correlation (DIC) is an optical technique that enables non-contact monitoring of displacement and strain fields. It operates by tracking two-dimensional or three-dimensional coordinates using random patterns. The measurements of the strain field and damage zone locations during bending were carried out using the digital image correlation (DIC) technique. The region of interest was rectangular with dimensions 100×40 mm^2, and it covered an area on the front side of the beam, between four PZT sensors. The inspected region was divided into facets of 19×19 pixels and a step of 16 pixels. The matching of digital images between the non-deform state and the subsequent states during

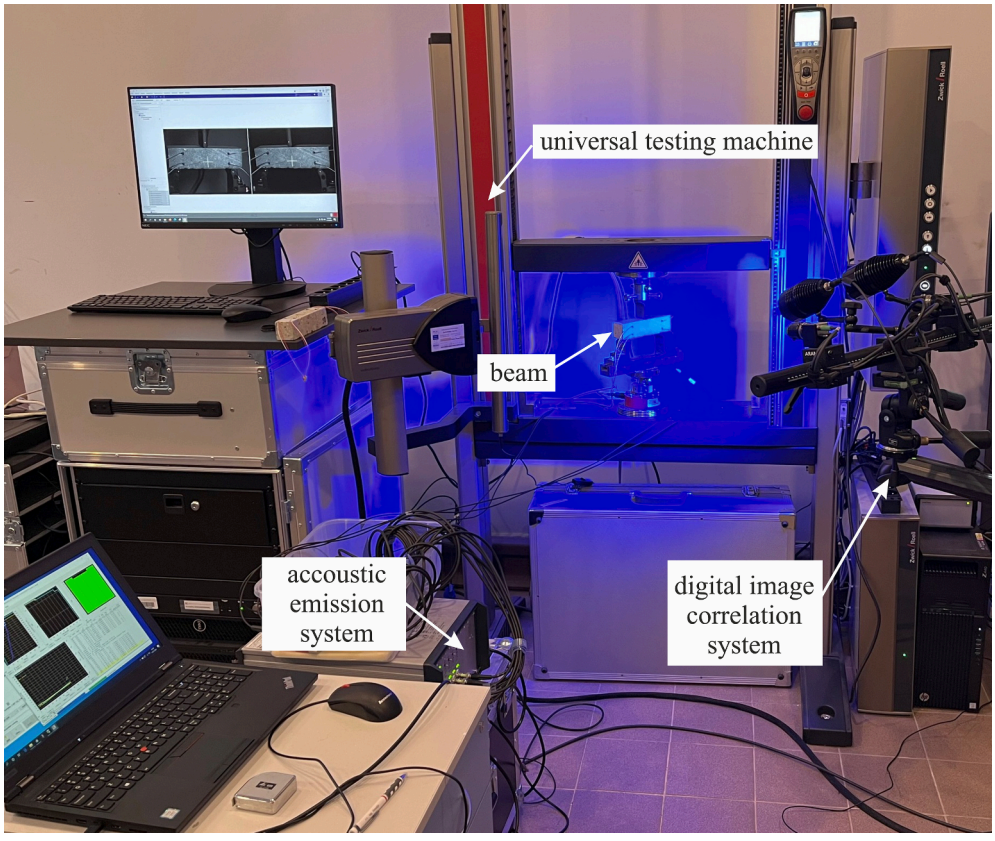

Fig. 3. Experimental setup.

mechanical degradation was calculated using the criterion of normalized zero-mean cross-correlation.

3.4. Acoustic emission

Acoustic emission refers to a phenomenon in which a transient elastic wave is immediately generated due to the rapid release of energy following material damage. These elastic waves are detected and recorded by AE sensors attached to the surface of the object and converted into electrical signals [30,31]. The commonly used characteristics of the AE signal are shown in Fig. 4, including the amplitude, energy, ringing counts and duration. In this paper, the crack evolution of concrete specimens under bending was investigated using typical AE characteristics such as the cumulative number of hits, peak amplitude, and three analysis methods including the b-value method, the Ib-value method, and the AE intensity analysis method which will be referred to below.

3.4.1. b-value method

The b-value analysis approach was originally used in earthquake engineering to quantify the seismic activity in the earth's strata and has been widely recognized by seismologists [32,33].The b-value approach can be used to explore the AE research area because the acoustic waves generated during AE events are comparable to seismic waves. For AE analysis, the Gutenberg-Richter (GR) law [33] of seismic wave analysis can be calculated as follows [34,35]:

$$\log_{10}N = a - b\left(\frac{A_{dB}}{20}\right) \tag{1}$$

where N is the number of AE hits with amplitudes greater than A_{dB}; A_{dB} is the AE hit amplitude; a denotes the intercept along the $\log_{10}N$ axis and b is the slope of the regression line plotted against A_{dB}.

3.4.2. Ib-value method

An improved approach to b-value analysis was introduced by T. Shiotani et al. [36] which is useful for the analysis of cement-based materials. This refinement is called the Ib-value method. It has been derived using statistical values of AE events and can be calculated using the formula:

$$Ib = \frac{\log_{10}N(\mu - \alpha_1\sigma) + (\mu + \alpha_2\sigma)}{(\alpha_1 + \alpha_2)\sigma} \tag{2}$$

where σ and μ are the standard deviations and the mean of the amplitude statistics in the AE event group;α_1 and α_2 are the user-defined coefficients related to the amplitude of AE events, ranging from − 1 to 1, depending on the lower and upper limits of amplitude distributions of the AE events. The Ib-value is quite sensitive and changes with a minor fracture, hence the parameter N is often set to 100 recent hits to monitor the small fracture events [37,38].

3.4.3. AE signal intensity analysis method

The damage level and integrity of concrete structures can be characterised using the intensity analysis of the AE signal, which takes into account the amplitude and duration [39]. The historical index (HI) and the severity index ($log_{10}S_r$) are the analysis methods based on the AE signal intensity, used to assess the damage intensity of concrete structures [40].The HI index measures the changes in the signal strength of the most recent AE events to all AE events throughout the fracture process. The $HI(t)$ is calculated by using the following equation:

$$HI(t) = \frac{N}{N-K}\frac{\sum_{i=K+1}^{N}S_{oi}}{\sum_{i=1}^{N}S_{oi}} \tag{3}$$

where N is the number of hits up to time t; S_{oi} is the signal strength of the i^{th} hit, and K is the empirical coefficient that depends on the number of AE hits, as shown in Table 3.

Severity (S_r) is defined as the average signal intensity for the J hits with the maximum numerical value of signal strength [41]. It can be calculated as follows:

$$S_r = \frac{1}{J}\sum_{i=1}^{J}S_{oi} \tag{4}$$

where S_r represents the severity index,S_{oi} is the i^{th}-largest signal strength, and J represents the empirical constant related to the material for concrete structures, as shown in Table 4.

4. Results

4.1. Bending test

Fig. 5 illustrates the load–deflection and load-time curves of all tested specimens. The peak load values were: 3283.80 N, 3651.72 N, 3579.73 N, 3923.59 N, 3756.3 N, for specimens made of PC, 0.3% PFRC, 0.6% PFRC, 0.3% SFRC, 0.6% SFRC, respectively. The mean value was 3639 N, the standard deviation (SD) was 236.95 N and the coefficient of

Table 3
K-parameter for concrete structure [39,40].

No. of hits (N)	≤50	51–200	201–500	≥501
K	Not applicable	N − 30	0.85 N	N − 75

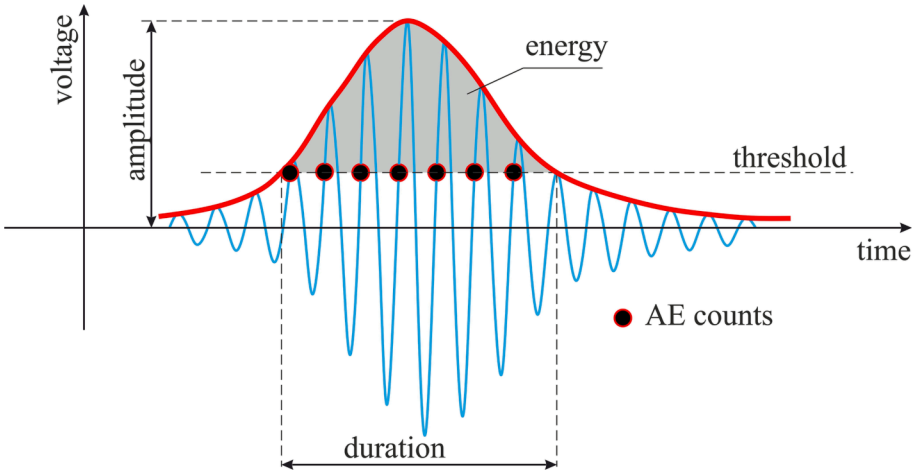

Fig. 4. The typical AE signal parameters.

Table 4
J value for concrete structures [39,40].

No. of hits (N)	<50	≥50
J	Not applicable	50

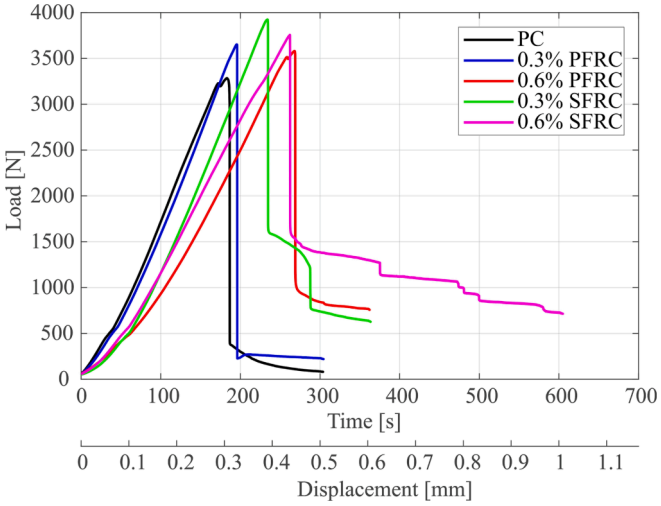

Fig. 5. Load-time and load–deflection-deflection curves of PC, PFRC and SFRC specimens.

variation (COV) was 6.51%. It can be observed, that the global maximum increased for the specimens made of mixtures containing the addition of polyolefin fibres (PS) and steel fibres (SF) in relation to the specimen made of plain concrete. The load–deflection curves for all specimens tested have a similar shape in a pre-peak region with an almost linear trend. They decreased sharply and exhibited a brittle failure after reaching the maximum flexural strength. However, the addition of reinforcing polyolefin and steel fibres to the plain concrete beams significantly improved the ductility and bending load capacity of the specimens. The load–deflection curve of the PFRC specimens dropped immediately after the maximum stress but then exhibited a gradual softening behaviour beyond this stage and towards the end of the test [42]. The SFRC specimens, on the other hand, significantly changed the post-crack behaviour of the load–deflection curves and improved the ductility performance as the load started to decrease. This is due to combined fibre-bridging effects between the steel and the surrounding matrix, which reduce macrocrack propagation and increase the post-peak residual strength [43,44].

4.2. Acoustic emission analysis

4.2.1. Characteristics of the distribution of cumulative AE hits

A characteristic of an AE hit is the number of AE signals registered by the AE sensor attached to the surface of the specimen. The response of the AE signals provides a quick indication of the behaviour of a material when it is subjected to stress. This behaviour is closely related to material durability, degradation, and failure. In this section, the fracture process of plain concrete specimens, as well as polyolefin fibre and steel

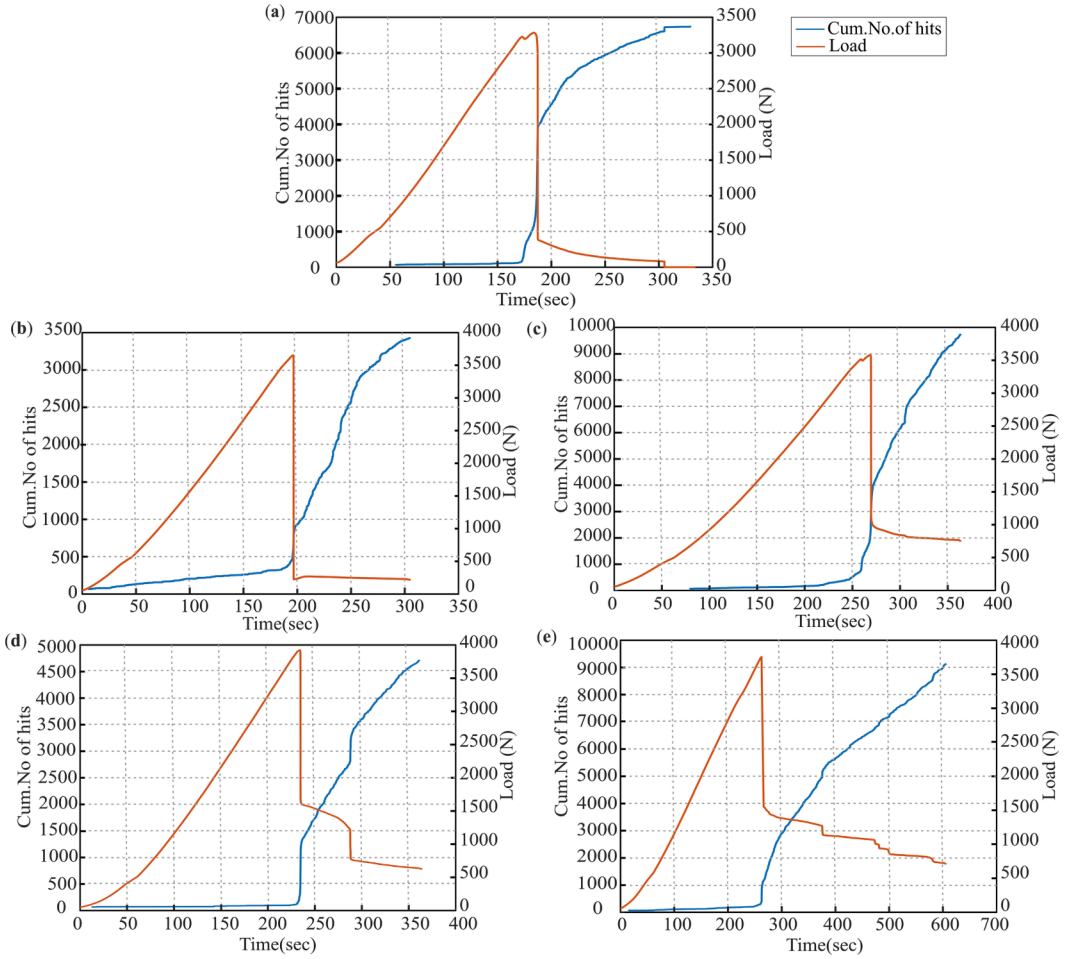

Fig. 6. Cumulative AE hits distribution diagram together with load-time curve: (a) PC; (b) 0.3% PFRC; (c) 0.6% PFRC; (d) 0.3% SFRC; and (e) 0.6% SFRC.

fibre reinforced concrete specimens, has been comprehensively analysed using the cumulative number of hits parameters. Fig. 6 depicts the cumulative number of AE hits along with the load-time curve for all tested specimens. It can be seen that the trend of the cumulative number of hits development profiles was almost the same for all the specimens tested. A small increase in the number of AE hits was recorded during the pre-peak stage. However, at the moment of peak load, the profiles of the cumulative AE hits increased sharply to the highest value when they reached their maximum crack strength. After the peak stage, the AE hit rate gradually decreased. Landis [45] found a similar pattern when examining micro–macro fracture correlations in concrete components employing AE hits activity. The fluctuation in the number of AE hits activity is clearly indicative of micro- and macrostructural changes caused by the development of cracks.

The cumulative number of AE hits profile of plain concrete reinforced with polyolefin fibres and steel fibres showed a significantly higher number of hits as the fibre aspect ratio increased from 0.3% to 0.6%, as shown in Fig. 6. This was mainly due to the responses of fibre pull-out events, which resulted in a considerably larger fracture surface area with increasing fibre content. As a result, more AE signals were generated. The cumulative number of AE hits profile of the plain concrete together with the load-time curve is shown in Fig. 6(a). It can be observed that there was considerably fewer hits recorded. The total number of AE hits activity of PFRC was lower than that of plain concrete when the fibre volume fraction is low (0.3%), as shown in Fig. 6(b). At a low fibre dosage of PF, the concrete matrix has fibre-free zones. The activity of the AE hits increases in the fibre-free areas as they are weaker and more prone to fracture. As the PFRC fibres were relatively short, they may not have been able to bridge these cracks, resulting in smaller AE hits than PC. However, as the fibre dosage increased from 0.3% to 0.6%, a higher number of AE hits was recorded for the PFRC, as shown in Fig. 6(c). This is because of the stronger fibre–matrix bonds, more evenly distributed fibres, and a greater bridging effect. As a result of these characteristics, the PFRC matrix demonstrated increased fracture resistance and slower crack propagation. The maximum cumulative number of AE hits was 9729 for the 0.6 %PF specimen, compared to 6740 for the plain concrete. As a result, the introduction of polyolefin fibers increased the effectiveness of crack growth inhibition, increasing the number of AE hits.

On the other hand, at a low dose of steel fibres in PC, as shown in Fig. 6(d), the total cumulative number of AE hits was higher than 0.3 % PF, being only 3430, compared to 4710. This is mainly because the hook-end shape and higher aspect ratio of the SF improved the bridging effect compared to the PF, resulting in increased stress redistribution and fracture propagation. This resulted in a higher AE activity than that of the PFRC. However, when the volume fraction of steel fibre was high, i.e.,0.6%, as shown in Fig. 6(e) the cumulative number of AE hits recorded was 9127 compared to 9729 for PFRC. This means that a slightly a lower number of fibre pull-out events was observed in the surrounding matrix compared to PFRC. A comparison of PFRC and SFRC shows that the ability of the steel fibres to bridge fractures is greater at the main crack, which increases the ability of the concrete matrix to bridge cracks at the microcrack level and retards crack propagation. In addition, the emission time of the AE signals and the crack load capacity of the SFRC specimens were higher than those of the PFRC specimens because of the stronger fibre–matrix bonds, uniformly distributed fibres, and a higher bridging effect, which improved the post-crack ductility and fracture toughness of the SFRC specimens. Based on the above analysis, it can be concluded that the AE method based on the hit activity can accurately define the meso- and macro-scale damage extent of the PFRC and SFRC specimens under bending.

4.2.2. Peak amplitude distribution of AE signals

In the study of fibre-reinforced composites, many researchers have used the amplitude function based on AE events to classify the different failure modes and strongly correlate with the crack sizes [46,47]. According to Aslan [47], the amplitude ranges of AE events between 40 and 60 dB are usually attributed to matrix cracking while AE event amplitudes ranging from 45 to 70 dB are responsible for fibre–matrix debonding, and the response amplitudes to fibre pullout and break vary from 60 to 100 dB. In this section, the crack magnitude of specimens made of plain concrete and concrete reinforced with polyolefin and steel fibres was comprehensively analysed using the peak amplitude distribution of AE events. The high density of AE amplitudes indicates the occurrence of a large number of AE hits. From Fig. 7, it can be observed that the distribution of the AE amplitude was almost similar to that of the AE hit activity and showed different cracking activity during the pre-peak, peak and post-peak load stages. As shown in Fig. 7(a), the AE amplitude data of plain concrete were monitored from 35 dB to 45 dB during the pre-peak stage, and the highest value (above 90 dB) of the AE amplitude was recorded during the peak loading stage. After the peak stage, AE amplitude values between 35 dB and 70 dB were observed, indicating that the aggregates have a limited role in fracture bridging.

The variations in the AE amplitude of the PFRC specimens during the pre-peak, peak and post-peak loading stages are shown in Fig. 7(b-c). In the pre-peak stage, AE amplitude values ranging from 35 to 60 dB were recorded, indicating that the microcracking activities reached their peak level due to the weaker fibre-free matrix zones leading to debonding.A maximum value of (98) of AE amplitude was achieved during the peak loading stage, indicating that the increased number of fibres available at the fractures induced fibre-fracture failure. However, AE amplitudes between 60 and 90 dB were recorded during the post-peak stage, which may be due to the greater number of fibre pull-out and sliding events from the matrix surface interface.

On the other hand, the values of the AE amplitude between 35 and 50 dB were recorded for the SFRC specimens as compared to the PFRC specimens during the pre-peak stage, as shown in Fig. 7(d-e). This was due to the presence of stronger fibre–matrix bond strength in the specimen, which prevented the growth and propagation of additional fractures. At the peak fracture stage, there was a significant increase in the AE amplitude (below 90 dB), which was lower than that of the PFRC specimen along the main crack formation path. This means that the crack load capacity of the SFRC specimens was higher than that of the PFRC specimens due to the higher fibre–matrix bonding strength and greater bridging effect. After the peak stage, the values of AE amplitudes between 60 dB and 90 dB were recorded, resulting in larger macrocracks due to greater fibre pull-out and sliding event behaviour between fibre–matrix interfaces [48].

4.2.3. b-value method

The b-value curves of plain, polyolefin fibre and steel fibre concrete beam specimens with fibre dosage of 0.3% and 0.6%, respectively, are shown alongside the load-time curves in Fig. 8. According to the conclusion of previous studies [34,49], when the b-value exceeded 1.0, it indicated that microcracks were dominant; when the b-value was 1.0, uniformly distributed macroscopic cracks to occurred in the specimens; when the b-value was < 1.0, the specimen was significantly damaged and contained large-scale macroscopic cracks. The damage state of all the tested specimens is shown in Fig. 8, together with load versus time curves. A noticeable fluctuation was observed in the b-value profiles of all the specimens tested during the whole loading stage, as shown in Fig. 8(b)-(e).

For the PFRC specimens, the b-value was greater during the pre-peak phases prior to the onset of major fracture. During the main fracture stage, the degree of fluctuation increased and then decreased after the peak stage. For the SFRC specimens, the b-value density was lower near the region of the major fracture stage, indicating that the fracture pattern changed from microcracks to macrocracks. After the peak stage, the b-value density was higher in the post-peak stage than in the peak stage. This was mainly due to the combined bridging behaviour between the steel fibre and concrete elements. As a result, the SFRC exhibited better post-crack ductility at fracture, resulting in improved sensitivity

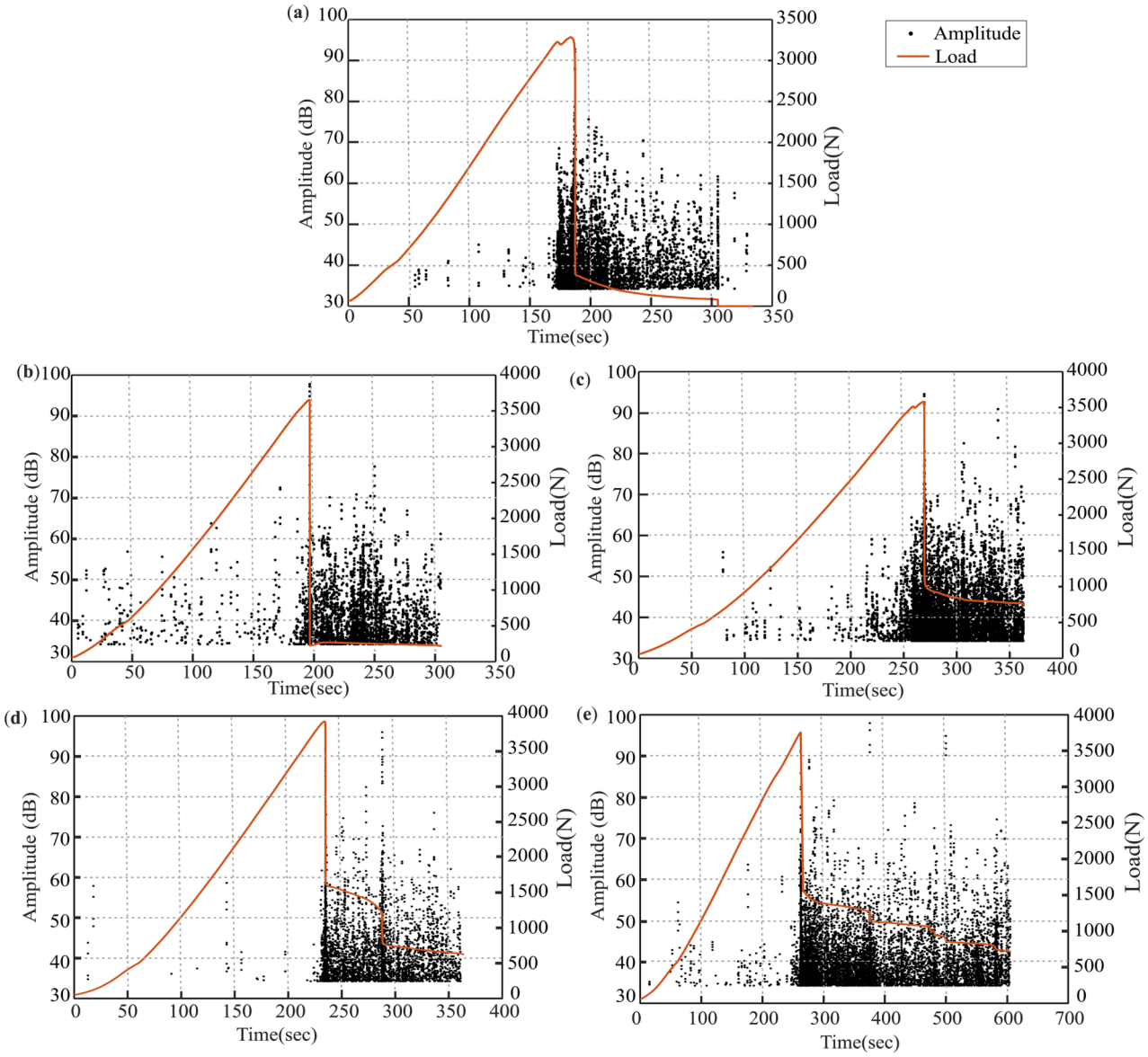

Fig. 7. AE peak amplitude distribution together with load-time curve: (a) PC; (b) 0.3 %PFRC; (c) 0.6 %PFRC; (d) 0.3% SFRC; and (e) 0.6% SFRC.

and bending capability. A comparison of the b-values of the PFRC and SFRC specimens revealed that the variation of the b-value and crack-growth rate of the SFRC specimens was much lower than that of the PFRC specimens. This indicates that the stronger fibre–matrix bonds, uniformly distributed fibres, and a higher bridging effect increased the post-cracking behaviour and inhibited the crack propagation of the SFRC specimens. The b-values of the PC, 0.3 %PF, and 0.6 %PF were determined from the b-value curve profile to be 0.814, 0.885, and 0.730, respectively. At the same time, 0.3 %SF and 0.6 %SF were found to be 0.868 and 0.583, respectively, at the moment of main crack formation. Table 5 summarises the maximum, minimum, and difference in b-values between the PFRC and SFRC specimens at the time of macroscopic crack initiation. A comparison of the b values of the PFRC and SFRC specimens shows that the fracture size of the SFRC specimens at the time of main crack initiation is significantly smaller than that of the PFRC specimens.

4.2.4. *Ib-value method*

The curves of the Ib-values of plain, polyolefin fibre and steel fibre concrete beam specimens with fibre dosage of 0.3% and 0.6%, respectively, are shown together with the load-time curves in Fig. 9. The Ib value of the AE is closely related to the propagation of microcracks and cracks within the material. Many studies have shown that a concrete structure with a higher Ib value during the fracture process releases more AE hits with smaller amplitudes that can develop into microscopic cracks. In contrast, the lower Ib-value produced fewer AE hits with larger amplitudes and the material was dominated by macroscale cracks [37,50]. Previous studies have suggested an Ib value of 0.05 as a threshold for predicting the condition of a material or structure [51,52]. In the current study, the Ib value was calculated by analysing the amplitude distribution of the last 100 hits collected during the fracture process.

It can be seen from Fig. 9 that the Ib values of all the specimens tested were relatively high during the pre-peak loading stage. This can be attributed to the high number of low-amplitude AE hits caused by the dominant microscopic cracks that occurred in the specimens. The decrease in the Ib value for the plain concrete during the pre-peak stage occurred significantly earlier than that for the PFRC and SFRC specimens, thus providing an early warning of severe damage (specimen cracking failure). The Ib-value decreased significantly as the load reached its peak, confirming the severe damage to the specimens due to the development of large-scale macrocracks at the moment of fracture. At low dosages of polyolefin fibre (0.3 %), AE events with higher Ib

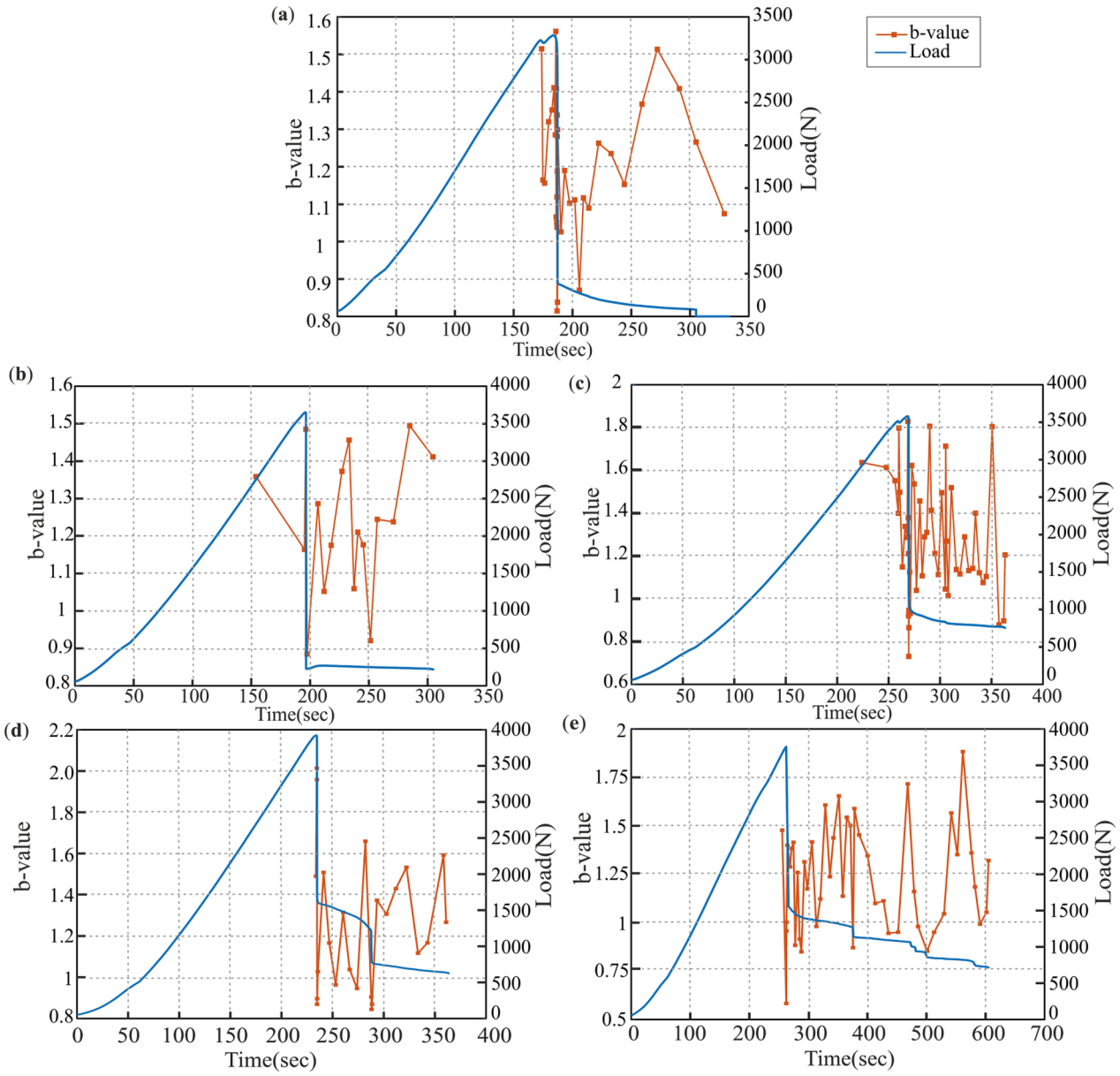

Fig. 8. B-value profiles together with load-time curve: (a) pc; (b) 0.3% pfrc; (c) 0.6% pfrc; (d) 0.3% sfrc; and (e) 0.6% sfrc.

Table 5
Maximum and minimum b-values for the main collapse stage.

Specimens	PC	0.3 % PFRC	0.6 % PFRC	0.3 % SFRC	0.6 % SFRC
Maximum b-value for the main collapse stage	1.561	1.485	1.828	2.013	1.477
Minimum b-value for the main collapse stage	0.814	0.885	0.730	0.868	0.583
Maximum-Minimum	0.747	0.6	1.098	1.145	0.894

values (0.075) were observed, indicating faster or unstable crack growth. At a high dosage of polyolefin fibre (0.6%), the AE events with smaller Ib-values (0.041) indicate that the fracture pattern shifted from micro- to macro-cracking. A similar trend of AE events with higher (0.073) and lower (0.042) Ib values was observed for SFRC with fibre dosage i.e., 0.3%, and 0.6%, respectively. The curves of the Ib values of the PFRC and SFRC specimens are consistent with the cumulative AE hits and peak amplitude graphs. In addition, the decrease in the Ib value of the SFRC specimens was smaller than that of the PFRC specimens during the main crack formation, which means that the addition of steel fibres to the plain concrete limited the crack growth and enhanced the cracking loading capacity. This shows that the presence of steel fibres in plain concrete favours the post-cracking softening behaviour and shows a gradual decrease in the strength of the specimens better than the PFRC specimens.

4.2.5. *AE signal intensity analysis method*

The damage characterisation of the plain concrete specimens, as well as the polyolefin fibre and steel fibre reinforced concrete specimens, was comprehensively analysed by intensity analysis (IA). Fig. 10 depicts the graphs of all specimens analysed using the historical index (HI) and logarithmic severity index (lg Sr) methods based on the AE signal intensity values (IA). Previous research has shown that a sudden rise in the HI-time curve and abrupt fluctuations in the lg Sr curve of the AE signal are associated with increased AE activity and serve as indicators of the severity of damage in concrete structures. Both changes are related to each other during crack development [51,18]. The onset of the damage

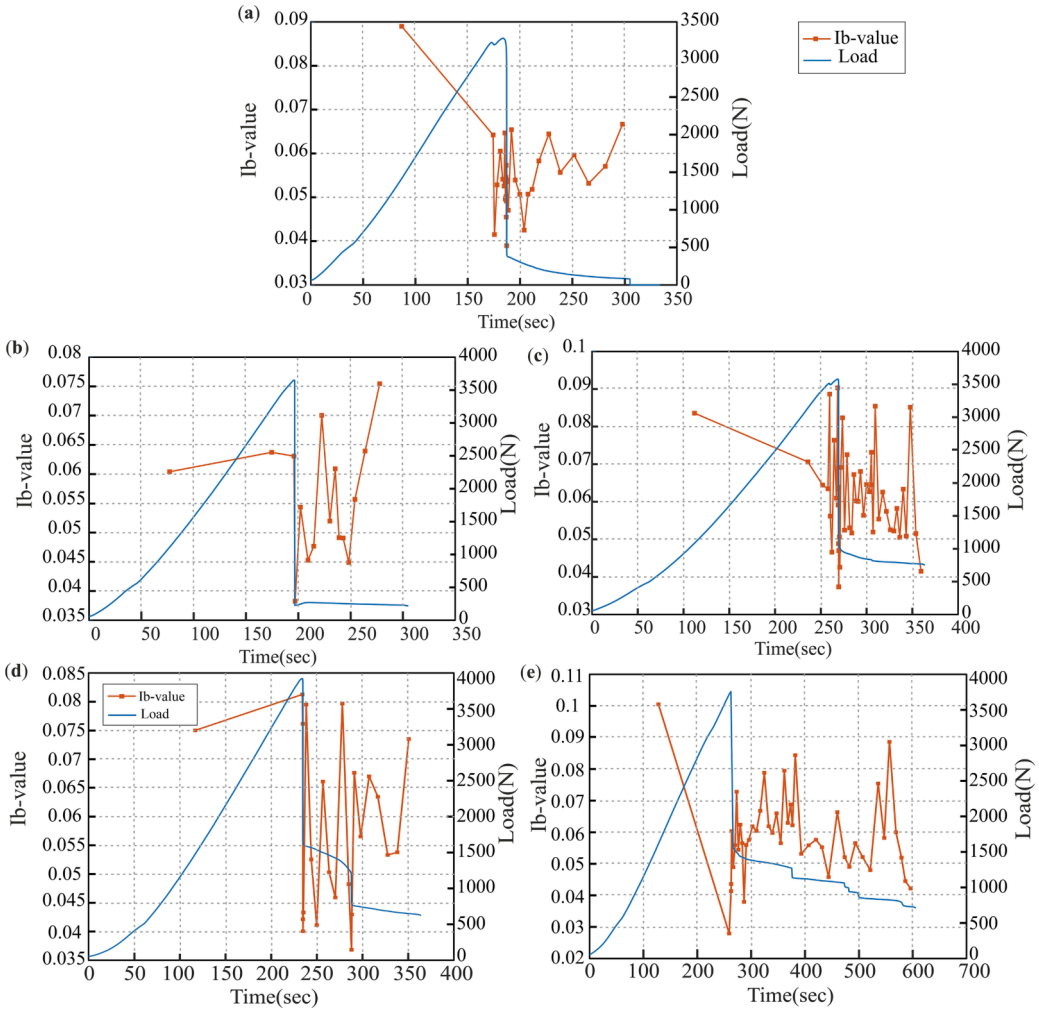

Fig.9. Ib-value profiles along with load-time curve: (a) PC; (b) 0.3% PFRC; (c) 0.6% PFRC; (d) 0.3% SFRC; and (e) 0.6% SFRC.

mechanism of all tested specimens was monitored using these two methods. A high peak in the historical index (HI) curve shows severe deterioration of the material, characterised by macroscopic cracking on a larger scale. As can be seen in Fig. 10(a), the HI-time curve for the PC specimen contains only one peak, which is nucleated at the main crack location (at 187 s) during the fracture process. The HI-time values of the PFRC specimens demonstrated an increasing trend with higher fibre dosages, ranging from 0.3% to 0.6%. In contrast, the HI-time values of the SFRC specimens exhibited an inverse correlation than PFRC specimens with increasing fibre dosages, ranging from 0.3% to 0.6%.

The addition of polyolefin fibres to plain concrete resulted in far fewer peaks throughout the fracture process than in the SFRC specimens. This indicates that in the PFRC specimens, due to the fibre-free matrix zones between the fibres and the surrounding matrix, macro-cracks with high signal intensity developed, and the degree of damage was high. The HI time peaks of the PFRC specimens, i.e. 0.3 %PF and 0.6 %PF, during the main crack formation were obtained at 196 s and 269 s, respectively, indicating that the fracture duration was slightly higher than that of the SFRC specimens. On the other hand, the incorporation of steel fibres into plain concrete resulted in lower HI-time curve values throughout the fracture process. This can be attributed to the improved crack-bridging ability of the steel fibres with the surrounding matrix at the microcrack level, resulting in a stronger matrix interface which delayed crack propagation and convergence. Each peak in the HI-time curve indicates the initiation of newly generated damage. The HI-time values of the SFRC specimens at dosages of 0.3% and 0.6% at the moment of major crack formation were at 234 s and 262 s, respectively. This means that the fracture duration of SFRC was slightly lower than that of PFRC and longer than that of PC. However, the HI-time curves of the SFRC specimens show fluctuations even after the emergence of macroscopic cracks, indicating a constant redistribution of shear stress between the fibre and matrix. This is due to the stronger fibre–matrix bond strength and greater bridging effect of the steel fibres available at the cracked surface for bridging the crack, which improves the post-crack ductility of the specimen and inhibits crack growth. The results of the HI-time peaks of the SFRC specimens are consistent with the damage evolution observed in the load versus time plot.

The damage characteristics of all the tested specimens can be determined from the abrupt position of the lg Sr curve in Fig. 10(b), which coincides with the maximum of the HI curve. The results show that the severity index values of the PFRC and SFRC were much higher than those of plain concrete. The PFRC specimens exhibited several AE knees during the fracture. However, fewer AE knees were observed in the SFRC specimens because of the higher bond strength between the matrix and steel fibres. The correlation between the historical index (HI) and severity index (lg Sr) values was used to assess the damage status of the PC, PFRC, and SFRC specimens (Fig. 10 (c)). The distance between the upper-right and lower-left corners determines the damage of the specimens corresponding to the AE signal source. The damage caused by an AE signal increases as the point approaches the upper-right corner and decreases as the point approaches the lower-left corner [53]. High HI and lg Sr values indicate that the specimen is at risk. Fig. 10(c) shows that the polyolefin fibre specimens are in hazardous conditions with a higher AE signal towards the upper right corner. However, the steel fibre

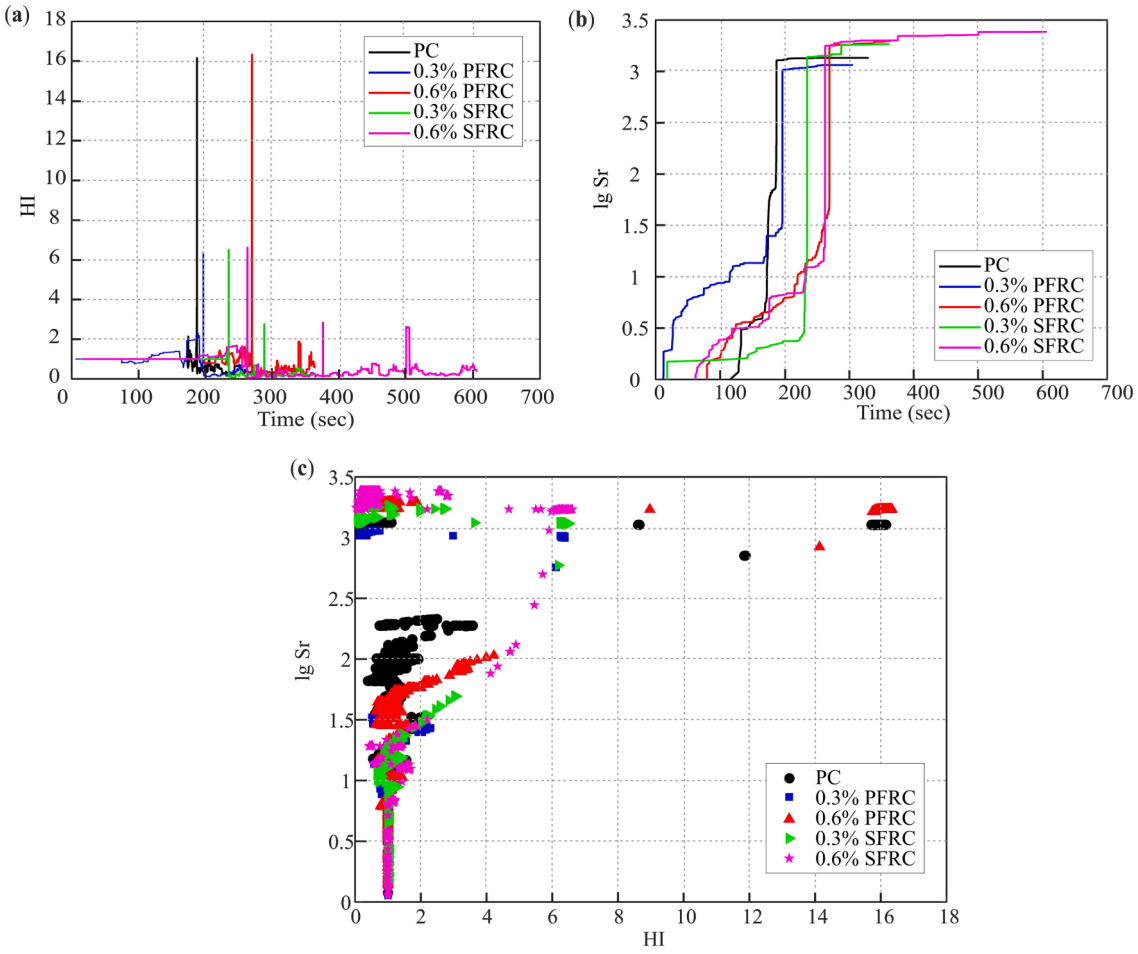

Fig. 10. AE intensity analysis of PC,PFRC and SFRC specimens: (a) HI curves; (b) lg Sr curves; and (c) HI vs. lg Sr.

specimens were located in the safe region, which was closer to the lower left corner. A comparison of the intensity analysis between the PFRC and SFRC specimens showed that the addition of steel fibres to the plain concrete caused less damage before failure and had better ductility after cracking.

4.3. *DIC visualization*

The DIC approach was used to investigate the fracture evolution of beams made of plain concrete, polyolefin fibre-reinforced concrete and steel fibre-reinforced concrete. In order to follow the progress of the fracture, the location of the damage zone and components of the lateral strain field at the surface of each specimen were determined. Fig. 11 depicts the horizontal strain ε_{xx} images created at various stress levels for a chosen area of interest (AOI). These images show the distribution of the strain throughout the AOI. The fracture evolution was identified at three characteristic time instances: 90% of the F_{max} before reaching the peak value (90% pre-F_{max}), the peak value (F_{max}), and the post-peak stage.

Examination of selected stages allowed the fracture progression of each specimen and its morphology to be monitored and followed. Fig. 11 shows that the pre-peak behaviour of the PFRC and SFRC specimens was similar, with a smaller damage zone height. However, as the load increased, the crack heights of the PFRC and SFRC specimens shifted upwards. After the peak, the crack developed over the entire length of the beam as the fibres were pulled out, leaving no fibres available to fill the cracks. For the PC specimen, the crack appeared at the peak load point. This crack caused the PC to fail catastrophically and the cracks propagated along the entire length of the beam.

When a low dosage of polyolefin fibre was introduced to the PC specimen (Fig. 11b), the first crack developed at approximately 90% of the pre-peak load value. This crack was followed by additional cracks close to the first crack as the applied load increased. The PFRC specimen with a higher concentration of polyolefin fibres showed a more regular crack pattern throughout the beam (Fig. 11c), indicating an effective crack-arresting mechanism. This indicates that when polyolefin fibres are added to plain concrete, the matrix of the fibre concrete cracks first, and the combined bridging behaviour of the fibre-surrounding matrix limits crack growth. In the post-peak softening segment, the crack length extended to the full beam height due to the debonding of the fibre pull-out responses at the matrix interface. On the other hand, the low dose of steel fibres in the PC sample showed a similar tendency to the PFRC sample, where the onset of micro-cracking appearance was observed at 90% pre-peak stress as shown in (Fig. 11d). The increased combined bridging behaviour and better fibre–matrix bonding prevented crack propagation as the stress level approached the ultimate strength, limiting the vertical propagation of the crack length. However, at a high dosage of SFRC (Fig. 11e), early microcracks appeared at approximately 90% of the peak pre-stress level at the top and bottom of the beam in the specimens. This finding suggests that the addition of steel fibres to ordinary concrete enhances the fibre–matrix contact, allowing microcracks to be bridged more efficiently [54]. At the post-peak stage, the fibres were entirely pulled out of the concrete matrix interfaces, and the fibres were not present to bridge the crack. Consequently, the crack height increased throughout the entire beam length.

According to the aforementioned DIC image analysis, it is worth noting that the crack length of the PC specimen was consistently greater than that of the PFRC and SFRC specimens across all loading stages. The

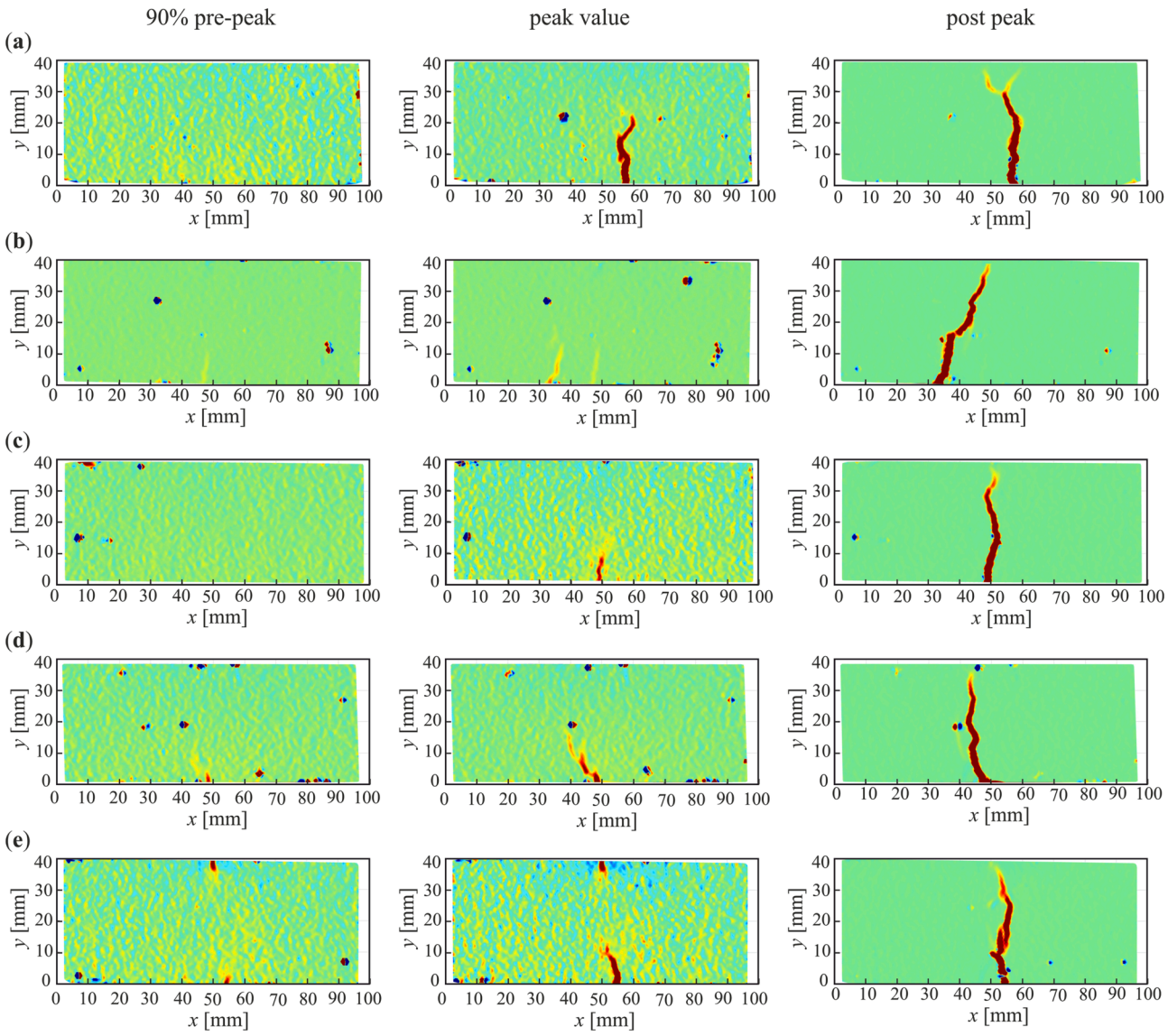

Fig. 11. Snapshots of lateral strain component ε_1 representing fracture evolution at different load levels: (a) PC; (b) 0.3% PFRC; (c) 0.6% PFRC; (d) 0.3% SFRC; and (e) 0.6% SFRC.

comparison of PFRC and SFRC showed that the SFRC specimens exhibited greater resistance at the post-peak stage than the PFRC specimens. This was attributed to the higher bond strength of SFRC and the uniform distribution of fibres with the surrounding interface, which enabled the effective bridging of macrocracks and crack growth inhibition. In SFRC, a greater number of fibres accessible at the crack surface promoted crack bridging, resulting in improved performance.

5. Discussion

5.1. Discussion on integration of AE and DIC data for damage localisation and evolution

This study aims to investigate the damage localisation and verify the fracture evolution of plain, PFRC and SFRC specimens by integrating the results obtained from AE fracture energies and the DIC technique. Extensive studies have shown that the local fracture energy is one of the most important parameters to characterize an AE event associated with fracture zones in concrete. The absolute AE energy related to the microcracking event was calculated by squaring the digitized AE recorded signal voltage and integrating the results during the event. During crack initiation, AE energy is emitted as an elastic wave and propagates from the crack location towards the specimen surface and can be detected by AE sensors. The source location of each AE event was determined based on the evaluation of the arrival time differences of the waves at each sensor and their respective sound velocities. Based on the arrival time difference of each sensor, a calculated velocity of 2000 m/s was used in this study. The AE events simultaneously recorded the damage changes in the specimens, and the acoustic events were plotted in 2D for comparison with the DIC results. Hyperbola diagrams are usually used for 2D planar localisation to verify the position of a selected point in 2D utilizing the location analyzer function of AE post-processing software [28,29].

Fig. 12 shows the 2D localisation maps of the AE events in terms of their AE fracture energies integrated with the DIC results. Three AE fracture energy levels were selected to identify the damage mechanism of the plain concrete, PFRC and SFRC specimens. From Fig. 12, it can be seen that AE events with lower energy are broader and more spread away from the macrocrack region of the specimens. The AE events with higher energy nucleated around the main splitting macrocracks path [55]. These high fracture energy AE events were located close to the centre of the localised damage zone, as shown in Fig. 12(a-e). The PFRC

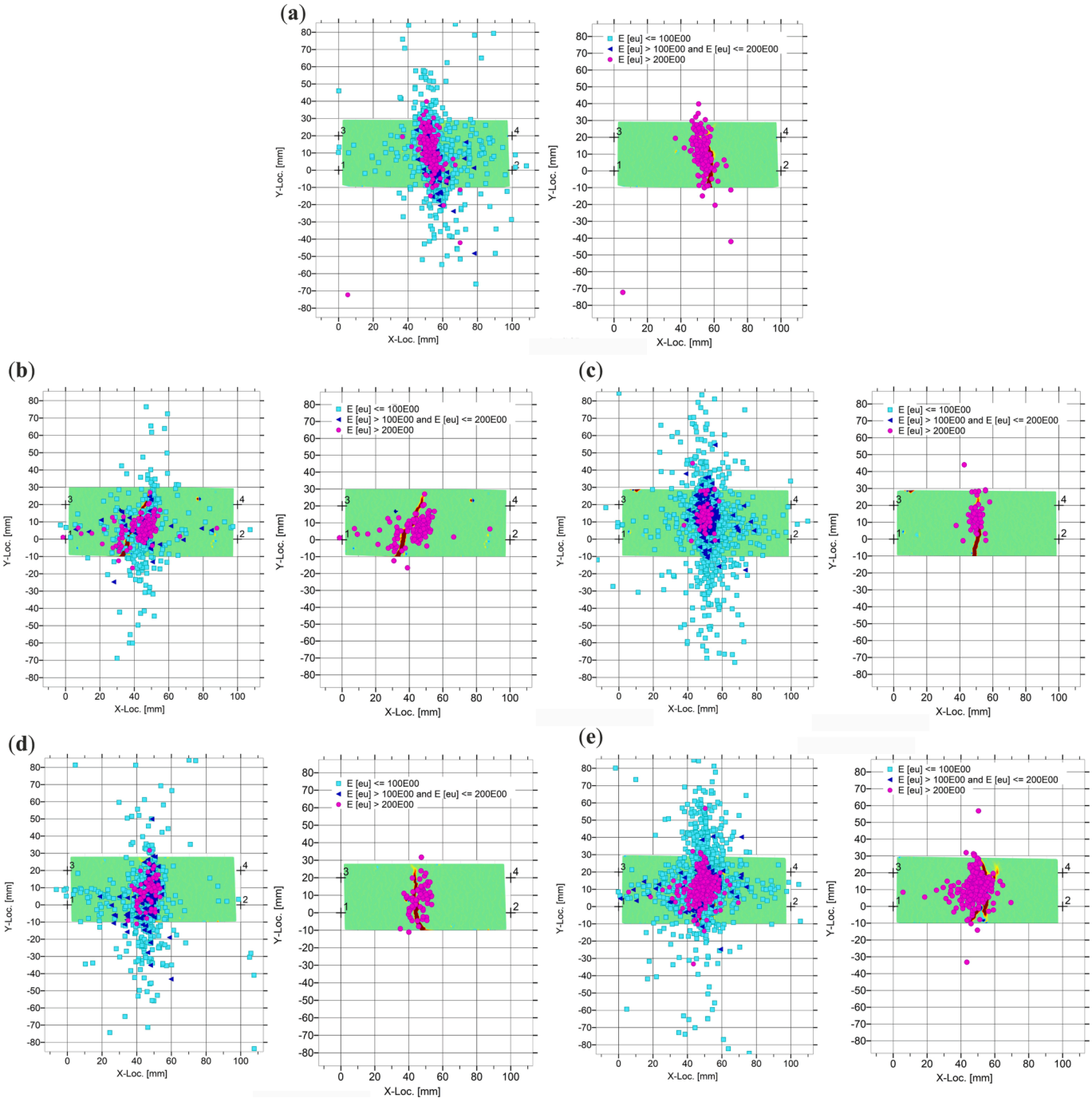

Fig. 12. 2D-localisation maps of AE Events as a function of fracture cumulative energies-integrated AE and DIC data: (a) PC; (b) 0.3% PFRC; (c) 0.6% PFRC; (d) 0.3% SFRC; and (e) 0.6% SFRC.

and SFRC specimens had an AE fracture energy value associated with a damage localisation area that was five times greater than that of the PC. Because PC has a lower tensile strength, it produces a larger damage zone. As a result, a larger damage zone area has less ability to prevent fracture propagation. However, the addition of polyolefin and steel fibres to PC strengthened the concrete and prevented fracture growth due to the smaller damage zone around the crack. As a result, higher AE fracture energy values correlate with a smaller damage zone. The higher amplitude, higher energy AE events are associated with the macrocrack and its dissipation mechanisms very close to the location of the primary collapse stage. A comparison of the PFRC and SFRC AE fracture energies showed that the AE fracture energies of the SFRC specimens were greater than those of the PFRC specimens. Because steel fibres provide a stronger fibre–matrix bond strength and an effective bridging mechanism than polyolefin fibres, they offer better reinforcement and fracture resistance. Therefore, SFRC fractures propagate locally through the reinforcing steel fibres, producing a higher AE fracture energy. However, polyolefin fibres have a lower tensile strength than steel fibres and therefore may not provide as much reinforcement and resistance to fracture propagation. As a result, the AE fracture energy generated in the PFRC was lower and the crack pattern was discontinuous. Based on the above analysis, it is concluded that the 2D localisation image of AE events with cumulative fracture energies of plain, PFRC, and SFRC specimens validates the fracture evolution, and their results are

consistent with the acoustic emission data.

5.2. Practical implementation of PFRC and SFRC

Fracture diagnostics and characterisation in PFRC and SFRC using combined AE and DIC techniques can detect micro-cracks, their locations and sizes, crack patterns, and fracture types. The results showed that, compared to polyolefin fibres, hook-end steel fibres improved crack resistance and reduced the likelihood of cracking in fibre-reinforced concrete at a maximum dosage of 0.6% relative to the total volume of concrete. This is due to the higher bridging effect with the surrounding matrices, uniformly dispersed fibres and stronger fibre–matrix bonding. This finding has important implications for the diagnosis and characterisation of fractures in PFRC and SFRC composites, as well as for the design and performance of these materials in the field. Some practical applications of PFRC and SFRC in both hot and cold environments have been presented.

Both PFRC and SFRC are useful in a wide range of applications due to their high strength, greater resistance to cracking, reduced shrinkage and improved durability. These properties make these materials ideal for use in both hot and cold environments. In hot climates, PFRC is preferred for applications such as airport runways, bridge decks and pavements where strong resistance to thermal expansion and contraction is required. Due to its high abrasion resistance, PFRC is suitable for use in car parks and industrial floors. However, SFRC is preferred for use in environments with temperature variations such as outdoor swimming pools, industrial floors and car parks. In colder regions, SFRC is preferred for retaining walls, runways and bridges due to its high resistance to freeze–thaw cycles. In addition to its strength, SFRC offers excellent resistance to cracking and frost heave caused by temperature changes, making it an excellent choice for use in cold climates. However, in cold climates, PFRC can be used for projects where excellent freeze–thaw resistance is required, such as retaining walls, concrete pipelines and foundations.

6. Conclusions

This study investigated the fracture evolution and detection of early cracking in PFRC and SFRC by using combined AE and DIC techniques. The focus of this study is to analyse the influence of fibre dosage on the post-cracking behaviour of PFRC vs. SFRC and their practical implementations in various concrete structures under different loading conditions. Moreover, the relationships between the source location of the AE events and AE fracture energies were investigated to verify the fracture evolution of the integrated AE and DIC data. The following conclusions were drawn.

1. The addition of steel fibres to plain concrete resulted in a greater improvement in the post-cracking behaviour of the load–deflection curves due to stronger fibre–matrix bonds and more effective fibre bridging than that of PFRC.
2. Based on the AE evaluation parameters, SFRC exhibited post-ductile behaviour, and the duration after the peak stage was longer than that of PFRC, indicating a higher ductility and crack arrest mechanism.
3. The b-value and Ib-value of the SFRC decreased rapidly before the peak load in the large fracture stage, indicating localised damage and impending macrocracking. At the end of the decrease in b-value due to the development of macrocracks. The b value increases significantly after macrocrack development, indicating that more dispersed microcracks are forming.
4. Based on the peak of HI and the abrupt increase in (lg Sr) AE intensity signal analysis, the PFRC specimens experienced more macrocracks with higher signal strength characteristics than the SFRC specimens. The correlation between the HI and lg Sr values demonstrated that the concrete specimens reinforced with steel fibres were characterised by a higher safety reserve.
5. The DIC maps revealed the initiation and development of micro-cracks in the fracture process zone. It was observed that at the peak load, the crack length of the PC specimen was significantly greater than that of the PFRC and SFRC specimens.
6. The integration of the AE and DIC data demonstrated that SFRC generated a larger AE fracture energy than PFRC due to its better crack arrest mechanism and fracture resistance.

The results obtained show that SFRC has better post-cracking behaviour and crack-arresting mechanism than PFRC and is a friendly alternative to normal concrete for use in hot and cold regions and to meet the goals of sustainable infrastructure.

CRediT authorship contribution statement

Shahzad Ashraf: Conceptualization, Formal analysis, Methodology, Software, Visualization, Writing – original draft. **Magdalena Rucka:** Conceptualization, Formal analysis, Funding acquisition, Investigation, Methodology, Project administration, Supervision, Writing – review & editing, Visualization.

Declaration of Competing Interest

The authors declare that they have no known competing financial interests or personal relationships that could have appeared to influence the work reported in this paper.

Data availability

Data will be made available on request.

Acknowledgements

The study was supported by the National Science Centre, Poland, project no. 2019/35/B/ST8/01905.

References

[1] D.Y. Yoo, Y.S. Yoon, A Review on Structural Behavior, Design, and Application of Ultra-High-Performance Fiber-Reinforced Concrete, Int. J. Concr. Struct. Mater. 10 (2016) 125–142, https://doi.org/10.1007/s40069-016-0143-x.
[2] N.M. Azmee, N. Shafiq, Ultra-high performance concrete: From fundamental to applications, Case Stud. Constr. Mater. 9 (2018), https://doi.org/10.1016/j.cscm.2018.e00197.
[3] V.C. Li, H. Stang, H. Krenchel, Micromechanics of crack bridging in fibre-reinforced concrete, Mater. Struct. 26 (1993) 486–494, https://doi.org/10.1007/BF02472808.
[4] E.A.H. Alwesabi, B.H.A. Bakar, I.M.H. Alshaikh, A.M. Zeyad, A. Altheeb, H. Alghamdi, Experimental investigation on fracture characteristics of plain and rubberized concrete containing hybrid steel-polypropylene fiber, Structures 33 (2021) 4421–4432, https://doi.org/10.1016/j.istruc.2021.07.011.
[5] P. Zhang, W. Wang, Y. Lv, Z. Gao, S. Dai, Effect of Polymer Coatings on the Permeability and Chloride Ion Penetration Resistances of Nano-Particles and Fibers-Modified Cementitious Composites, Polymers (Basel). 14 (2022), https://doi.org/10.3390/polym14163258.
[6] H. Ren, T. Li, J. Ning, S. Song, Analysis of damage characteristics of steel fiber-reinforced concrete based on acoustic emission, Eng. Fail. Anal. 148 (2023), 107166, https://doi.org/10.1016/j.engfailanal.2023.107166.
[7] B. Liu, J. Guo, X. Wen, J. Zhou, Z. Deng, Study on flexural behavior of carbon fibers reinforced coral concrete using digital image correlation, Constr. Build. Mater. 242 (2020), 117968, https://doi.org/10.1016/j.conbuildmat.2019.117968.
[8] V.M. de Alencar Monteiro, L.R. Lima, F. de Andrade Silva, On the mechanical behavior of polypropylene, steel and hybrid fiber reinforced self-consolidating concrete, Constr. Build. Mater. 188 (2018) 280–291, https://doi.org/10.1016/j.conbuildmat.2018.08.103.
[9] K. Hrabová, J. Láník, P. Lehner, Statistical and Practical Evaluation of the Mechanical and Fracture Properties of Steel Fibre Reinforced Concrete, Buildings. 12 (2022) 1082, https://doi.org/10.3390/buildings12081082.
[10] F. He, L. Biolzi, V. Carvelli, P.J.M. Monteiro, Digital imaging monitoring of fracture processes in hybrid steel fiber reinforced concrete, Compos. Struct. 298 (2022), 116005, https://doi.org/10.1016/j.compstruct.2022.116005.
[11] A. Karimipour, M. Edalati, J. de Brito, Biaxial mechanical behaviour of polypropylene fibres reinforced self-compacting concrete, Constr. Build. Mater. 278 (2021), https://doi.org/10.1016/j.conbuildmat.2021.122416.

[12] M.M. Moein, A. Saradar, K. Rahmati, Y. Rezakhani, S.A. Ashkan, M. Karakouzian, Reliability analysis and experimental investigation of impact resistance of concrete reinforced with polyolefin fiber in different shapes, lengths, and doses, J. Build. Eng. 69 (2023), 106262, https://doi.org/10.1016/j.jobe.2023.106262.
[13] M. Khan, M. Ali, Use of glass and nylon fibers in concrete for controlling early age micro cracking in bridge decks, Constr. Build. Mater. 125 (2016) 800–808, https://doi.org/10.1016/j.conbuildmat.2016.08.111.
[14] K. Cui, L. Xu, T. Tao, L. Huang, J. Li, J. Hong, H. Li, Mechanical behavior of multiscale hybrid fiber reinforced recycled aggregate concrete subject to uniaxial compression, J. Build. Eng. 71 (2023), 106504, https://doi.org/10.1016/j.jobe.2023.106504.
[15] M. Szelag, Evaluation of cracking patterns in cement composites-from basics to advances: A review, Materials (Basel). 13 (2020), https://doi.org/10.3390/ma13112490.
[16] Q. Lin, B. Wan, Y. Wang, Y. Lu, J.F. Labuz, Unifying acoustic emission and digital imaging observations of quasi-brittle fracture, Theor. Appl. Fract. Mech. 103 (2019), https://doi.org/10.1016/j.tafmec.2019.102301.
[17] R. Kravchuk, E.N. Landis, Acoustic emission-based classification of energy dissipation mechanisms during fracture of fiber-reinforced ultra-high-performance concrete, Constr. Build. Mater. 176 (2018) 531–538, https://doi.org/10.1016/j.conbuildmat.2018.05.039.
[18] S. Ashraf, S. Khan, V.K. Oad, Microcracking monitoring and damage detection of graphene nanoplatelets-cement composites based on acoustic emission technology, Case Stud. Constr. Mater. 18 (2023) e01844.
[19] M. Rucka, E. Wojtczak, M. Knak, M. Kurpińska, Characterization of fracture process in polyolefin fibre-reinforced concrete using ultrasonic waves and digital image correlation, Constr. Build. Mater. 280 (2021), https://doi.org/10.1016/j.conbuildmat.2021.122522.
[20] E. Wojtczak, M. Rucka, Ł. Skarżyński, Monitoring the fracture process of concrete during splitting using integrated ultrasonic coda wave interferometry, digital image correlation and X-ray micro-computed tomography, NDT E Int. 126 (2022), https://doi.org/10.1016/j.ndteint.2021.102591.
[21] L. Xu, B. Li, X. Ding, Y. Chi, C. Li, B. Huang, Y. Shi, Experimental Investigation on Damage Behavior of Polypropylene Fiber Reinforced Concrete under Compression, Int. J. Concr. Struct. Mater. 12 (2018), https://doi.org/10.1186/s40069-018-0302-3.
[22] D. Logoń, K. Schabowicz, The recognition of the micro-events in cement composites and the identification of the destruction process using acoustic emission and sound spectrum, Materials (Basel). 13 (2020) 1–13, https://doi.org/10.3390/ma13132988.
[23] D. Logoń, Identification of the destruction process in Quasi Brittle concrete with dispersed fibers based on acoustic emission and sound spectrum, Materials (Basel). 12 (2019), https://doi.org/10.3390/ma12142266.
[24] D.G. Aggelis, D.V. Soulioti, E.A. Gatselou, N.M. Barkoula, T.E. Matikas, Monitoring of the mechanical behavior of concrete with chemically treated steel fibers by acoustic emission, Constr. Build. Mater. 48 (2013) 1255–1260, https://doi.org/10.1016/j.conbuildmat.2012.06.066.
[25] B. Cai, K. Li, F. Fu, Flexural behavior of steel fiber-reinforced coal gangue aggregate concrete beams, Structures. 52 (2023) 131–145, https://doi.org/10.1016/j.istruc.2023.03.172.
[26] Ł. Skarżyński, J. Suchorzewski, Mechanical and fracture properties of concrete reinforced with recycled and industrial steel fibers using Digital Image Correlation technique and X-ray micro computed tomography, Constr. Build. Mater. 183 (2018) 283–299, https://doi.org/10.1016/j.conbuildmat.2018.06.182.
[27] S.Y. Alam, A. Loukili, F. Grondin, E. Rozière, Use of the digital image correlation and acoustic emission technique to study the effect of structural size on cracking of reinforced concrete, Eng. Fract. Mech. 143 (2015) 17–31, https://doi.org/10.1016/j.engfracmech.2015.06.038.
[28] A. Boniface, J. Saliba, Z.M. Sbartaï, N. Ranaivomanana, J.P. Balayssac, Evaluation of the acoustic emission 3D localisation accuracy for the mechanical damage monitoring in concrete, Eng. Fract. Mech. 223 (2020), https://doi.org/10.1016/j.engfracmech.2019.106742.
[29] W. Zhou, Z.H. Lv, Z.Y. Li, X. Song, Acoustic emission response and micro-deformation behavior for compressive buckling failure of multi-delaminated composites, J. Strain Anal. Eng. Des. 51 (2016) 397–407, https://doi.org/10.1177/0309324716645244.
[30] J. Xu, S. Ashraf, S. Khan, X. Chen, A. Akbar, F. Farooq, Micro-cracking pattern recognition of hybrid CNTs/GNPs cement pastes under three-point bending loading using acoustic emission technique, J. Build. Eng. 42 (2021), https://doi.org/10.1016/j.jobe.2021.102816.
[31] J. Geng, Q. Sun, Y. Zhang, L. Cao, W. Zhang, Studying the dynamic damage failure of concrete based on acoustic emission, Constr. Build. Mater. 149 (2017) 9–16, https://doi.org/10.1016/j.conbuildmat.2017.05.054.
[32] Z.H. El-Isa, D.W. Eaton, Spatiotemporal variations in the b-value of earthquake magnitude-frequency distributions: Classification and causes, Tectonophysics. 615–616 (2014) 1–11, https://doi.org/10.1016/j.tecto.2013.12.001.
[33] Q. Han, L. Wang, J. Xu, A. Carpinteri, G. Lacidogna, A robust method to estimate the b-value of the magnitude-frequency distribution of earthquakes, Chaos, Solitons and Fractals. 81 (2015) 103–110, https://doi.org/10.1016/j.chaos.2015.09.004.
[34] I.S. Colombo, I.G. Main, M.C. Forde, Assessing Damage of Reinforced Concrete Beam Using " b -value" Analysis of Acoustic Emission Signals, J. Mater. Civ. Eng. 15 (2003) 280–286, https://doi.org/10.1061/(asce)0899-1561(2003)15:3(280).
[35] A. Carpinteri, G. Lacidogna, S. Puzzi, From criticality to final collapse: Evolution of the "b-value" from 1.5 to 1.0, Chaos, Solitons and Fractals. 41 (2009) 843–853, https://doi.org/10.1016/j.chaos.2008.04.010.
[36] T. Shiotani, M. Ohtsu, K. Ikeda, Detection and evaluation of AE waves due to rock deformation, Constr. Build. Mater. 15 (2001) 235–246, https://doi.org/10.1016/S0950-0618(00)00073-8.
[37] D. Jung, W.R. Yu, W. Na, Use of acoustic emission b(Ib)-values to quantify damage in composites, Compos. Commun. 22 (2020), 100499, https://doi.org/10.1016/j.coco.2020.100499.
[38] D.G. Aggelis, D.V. Soulioti, N. Sapouridis, N.M. Barkoula, A.S. Paipetis, T. E. Matikas, Acoustic emission characterization of the fracture process in fibre reinforced concrete, Constr. Build. Mater. 25 (2011) 4126–4131, https://doi.org/10.1016/j.conbuildmat.2011.04.049.
[39] M.N. Noorsuhada, An overview on fatigue damage assessment of reinforced concrete structures with the aid of acoustic emission technique, Constr. Build. Mater. 112 (2016) 424–439, https://doi.org/10.1016/j.conbuildmat.2016.02.206.
[40] D. Li, Z. Chen, Q. Feng, Y. Wang, Damage analysis of CFRP-confined circular concrete-filled steel tubular columns by acoustic emission techniques, Smart Mater. Struct. 24 (2015), https://doi.org/10.1088/0964-1726/24/8/085017.
[41] A. Nair, Acoustic emission monitoring and quantitative evaluation of damage in reinforced concrete members and bridges, Louisiana State University and Agricultural & Mechanical College, 2006.
[42] R. Babaie, M. Abolfazli, A. Fahimifar, Mechanical properties of steel and polymer fiber reinforced concrete, J. Mech. Behav. Mater. 28 (2020) 119–134, https://doi.org/10.1515/jmbm-2019-0014.
[43] A. Benedetto, L. Pajewski, Springer Transactions in Civil and Environmental Engineering, 2015.
[44] F. Liu, W. Ding, Y. Qiao, Experimental investigation on the flexural behavior of hybrid steel-PVA fiber reinforced concrete containing fly ash and slag powder, Constr. Build. Mater. 228 (2019), https://doi.org/10.1016/j.conbuildmat.2019.116706.
[45] E.N. Landis, Micro–macro fracture relationships and acoustic emissions in concrete, Constr. Build. Mater. 13 (1999) 65–72, https://doi.org/10.1016/S0950-0618(99)00009-4.
[46] N. Chandarana, D.M. Sanchez, C. Soutis, M. Gresil, Early damage detection in composites during fabrication and mechanical testing, Materials (Basel). 10 (2017), https://doi.org/10.3390/ma10070685.
[47] M. Aslan, Investigation of damage mechanism of flax fibre LPET commingled composites by acoustic emission, Compos. Part B Eng. 54 (2013) 289–297, https://doi.org/10.1016/j.compositesb.2013.05.042.
[48] B. Li, L. Xu, Y. Shi, Y. Chi, Q. Liu, C. Li, Effects of fiber type, volume fraction and aspect ratio on the flexural and acoustic emission behaviors of steel fiber reinforced concrete, Constr. Build. Mater. 181 (2018) 474–486, https://doi.org/10.1016/j.conbuildmat.2018.06.065.
[49] T. Schumacher, C.C. Higgins, S.C. Lovejoy, Estimating operating load conditions on reinforced concrete highway bridges with b-value analysis from acoustic emission monitoring, Struct. Heal. Monit. 10 (2011) 17–32, https://doi.org/10.1177/1475921710365424.
[50] I.M. De Rosa, C. Santulli, F. Sarasini, Acoustic emission for monitoring the mechanical behaviour of natural fibre composites: A literature review, Compos. Part A Appl. Sci. Manuf. 40 (2009) 1456–1469, https://doi.org/10.1016/j.compositesa.2009.04.030.
[51] Q. Han, G. Yang, J. Xu, Z. Fu, G. Lacidogna, A. Carpinteri, Acoustic emission data analyses based on crumb rubber concrete beam bending tests, Eng. Fract. Mech. 210 (2019) 189–202, https://doi.org/10.1016/j.engfracmech.2018.05.016.
[52] D.G. Aggelis, T. Shiotani, S. Momoki, A. Hirama, Acoustic emission and ultrasound for damage characterization of concrete elements, ACI Mater. J. 106 (2009) 509–514. 10.14359/51663333.
[53] X. Xu, Z. Jin, Y. Yu, N. Li, Damage source and its evolution of ultra-high performance concrete monitoring by digital image correlation and acoustic emission technologies, J. Build. Eng. 65 (2023), 105734, https://doi.org/10.1016/j.jobe.2022.105734.
[54] S. Muralidhara, B.K.R. Prasad, H. Eskandari, B.L. Karihaloo, Fracture process zone size and true fracture energy of concrete using acoustic emission, Constr. Build. Mater. 24 (2010) 479–486, https://doi.org/10.1016/j.conbuildmat.2009.10.014.
[55] A. Bakour, M. Ben Ftima, A. Chéruel, Combination of acoustic emission and digital image correlation monitoring for wedge splitting tests on large concrete specimens, Constr. Build. Mater. 322 (2022), https://doi.org/10.1016/j.conbuildmat.2022.126496.